Journal of Alloys and Compounds 509S (2011) S616–S620

Contents lists available at ScienceDirect

Journal of Alloys and Compounds

journal homepage: www.elsevier.com/locate/jallcom

Microstructure and hydrogen storage capacity of magnesium hydride with zirconium and niobium fluoride additives after cyclic loading

I.E. Malka [a,*], J. Bystrzycki [a], T. Płociński [b], T. Czujko [a]

[a] Department of Advanced Materials and Technology, Military University of Technology, 2 Kaliskiego Str., 00-908 Warsaw, Poland
[b] Faculty of Materials Science and Engineering, Warsaw University of Technology, 141 Wołoska Str., 02-507 Warsaw, Poland

ARTICLE INFO

Article history:
Received 23 July 2010
Received in revised form 13 October 2010
Accepted 22 October 2010
Available online 4 November 2010

Keywords:
Magnesium hydride
Metal halides
Cyclic hydriding/dehydriding
Microstructure
Hydrogen storage capacity

ABSTRACT

In this work, new results on the microstructure and hydrogen storage capacity of MgH_2 with ZrF_4 and NbF_5 after cyclic loading are presented. Commercial MgH_2 powder was mixed with 7 wt.% metal halide powder and subsequently ball milled in an inert atmosphere. The microstructure of the powders was investigated with high-resolution SEM using BSE/STEM/EDS detectors. The thin samples were prepared by FIB. The materials exhibited good reversibility and hydrogen sorption stability. However, the hydrogen storage capacity decreased in both materials after prolonged cycling at 325 °C. Better sorption stability was observed for MgH_2 with ZrF_4 than for MgH_2/NbF_5. Its microstructure consisted of an MgH_2 matrix and stable nano-sized ZrF_4 particles embedded in the "core" structure of the particles. The outer layer of the particles was identified as MgH_2.The gradual decrease in the hydrogen storage capacity while cyclic loading for this particular material is due to some stabilization of the fraction of MgH_2/Mg with continues increase of grain size in the MgH_2/Mg regions, from about 10 nm after ball milling to hundreds of nanometers after cycling. The stabilization process makes a fraction of MgH_2/Mg inactive in the process of hydrogen desorption/absorption. In contrast, the MgH_2/NbF_5 sample after cyclic loading exhibited an MgH_2/Mg matrix with some amount of MgF_2 phase and nano-sized Nb-rich precipitates. The formation of the MgF_2 phase is mainly responsible for the lost of hydrogen storage capacity of the MgH_2/NbF_5 sample while cyclic loading.

1. Introduction

Magnesium hydride (MgH_2) is a promising material for reversible gaseous hydrogen storage because it has high gravimetric (7.6 wt.%) and volumetric (110 kg m^{-3}) hydrogen storage densities. Magnesium is abundant, inexpensive and environmentally benign. Unfortunately, due to its hydride stability and slow hydrogen sorption kinetics, the actual application of Mg as a hydrogen storage material is limited [1].

In the last decade, it has been clearly shown that the sorption properties of Mg can be essentially improved by reducing the particle and grain sizes as well as by forming composite structures with low-temperature hydrides [1,2]. Catalyst additives such as pure transition metals and their oxides as well as intermetallic compounds are also powerful means of improving hydrogen sorption kinetics [1,2]. Among various additives, metal halides often present even better catalytic activity than their corresponding metal constituents or metal oxides. For example, Bhat et al. [3] compared the effect of the oxide catalysts Nb_2O_5 with its halide counterpart, $NbCl_5$. They found a higher catalytic activity for $NbCl_5$ as compared to Nb_2O_5, indicating that neither oxide ion nor transition metal cation is crucial for hydrogen sorption. Additionally, the authors proved that the ionicity of the catalyst is important in enhancing the sorption kinetics of MgH_2.

There are different possible reactions of Mg (or MgH_2) with metal halides while ball milling and then cyclically hydriding/dehydriding [3–9]. In a previous study [10], we showed that additives of different halides possessing the highest state of oxidation reduce the magnesium hydride decomposition temperature more effectively than their counterparts with lower oxidation states. Among different metal halides, the ZrF_4 and NbF_5 additives showed the most significant influences on the desorption temperature and the sorption kinetics of MgH_2. In the present work, we report the results of studies on the microstructure and hydrogen storage capacity of MgH_2 with both ZrF_4 and NbF_5 additives after cyclic loading.

2. Experimental procedure

Commercial MgH_2 powders (Alfa Aesar, 99.8% purity) with 7 wt.% NbF_5 and ZrF_4 (Sigma–Aldrich) were mechanically (ball) milled using a Fritsch P6 planetary mill for 1 h under high purity argon. The total mass of each MgH_2–halide powder mixture was 5 g. All powder samples were loaded with thirty 10-mm-diameter balls

* Corresponding author. Tel.: +48 22 683 7693; fax: +48 22 683 9445.
E-mail address: imalka@wat.edu.pl (I.E. Malka).

0925-8388/$ – see front matter © 2010 Elsevier B.V. All rights reserved.
doi:10.1016/j.jallcom.2010.10.122

into an 80-ml vial of stainless steel under argon of min. purity of 99.999% (H_2O and O < 1 ppm). The ball-to-powder weight ratio was ~25, and the rotation speed of the milling vial was 650 rpm. All handling of the powders, before and after milling, was conducted in a Labmaster Glovebox Workstation (MBraun) under a continuously purified argon atmosphere. The amounts of oxygen and water were below 0.1 ppm.

To determine the cycle performance of the hydrogen sorption kinetics and the relative degradation of the hydrogen storage capacity, the hydriding–dehydriding steps were repeated up to 50 cycles using an automated Sieverts' apparatus (HTP1-S, Hiden Isochema). The samples were first desorbed in vacuum and then hydrogenated under 10 bar of hydrogen pressure (99.9999% purity). Both processes were carried out for 10 min at 325 °C. This time was sufficient to reach completeness of absorption and desorption processes.

The microstructures of the MgH_2/halide samples after cyclic loading were examined with a high-resolution field emission scanning electron microscope (FE SEM) (HITACHI S5500) equipped with a backscattered electron detector (BSE), an energy dispersive X-ray spectrometer (EDS) and a duo-STEM bright/dark field detector. Because the investigated samples included both nano- and microcrystalline structures, thin foils for electron microscopy were prepared by the focused ion beam (FIB) technique using the FB-2100 Hitachi system. A liquid ion metal source was used as the source of the gallium ion beam, and the accelerating voltage used was 40 kV. Tungsten was used as a protective layer.

The X-ray diffraction patterns for all of the investigated powder samples were recorded with a Rigaku Ultima IV diffractometer using CuK_α radiation with the operating parameters of 40 mA and 40 kV. The scanning speed was 5°/min with the step size of 0.02°.

It is to be pointed out that the powder samples for investigations in FE SEM and X-ray diffractometer were simply mounted in the respective holders in air without using any dedicated environmental holders. In order to prevent a spontaneous burning of the material which occurs when it is exposed to air after removing it from the Sieverts' apparatus the samples for microscopic and XRD observations were first very slowly exposed to air and then transferred to a microscope or an X-ray diffractometer. Therefore, some amount of oxygen in all investigated samples can be found as will be discussed in the following sections.

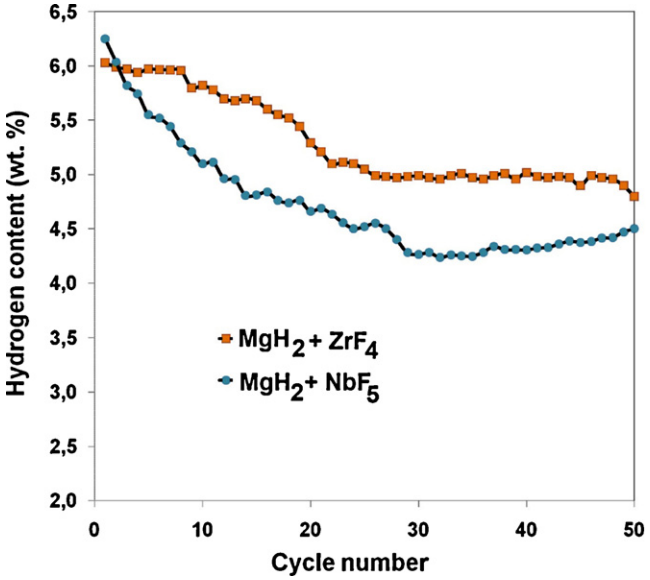

Fig. 1. Hydrogen storage capacity as a function of sorption cycle number.

3. Results and discussion

The cycle performance of MgH_2 with the NbF_5 and ZrF_4 additives at 325 °C is shown in Fig. 1. The hydrogen storage capacity of the MgH_2/ZrF_4 sample decreases slightly with cycling and reaches

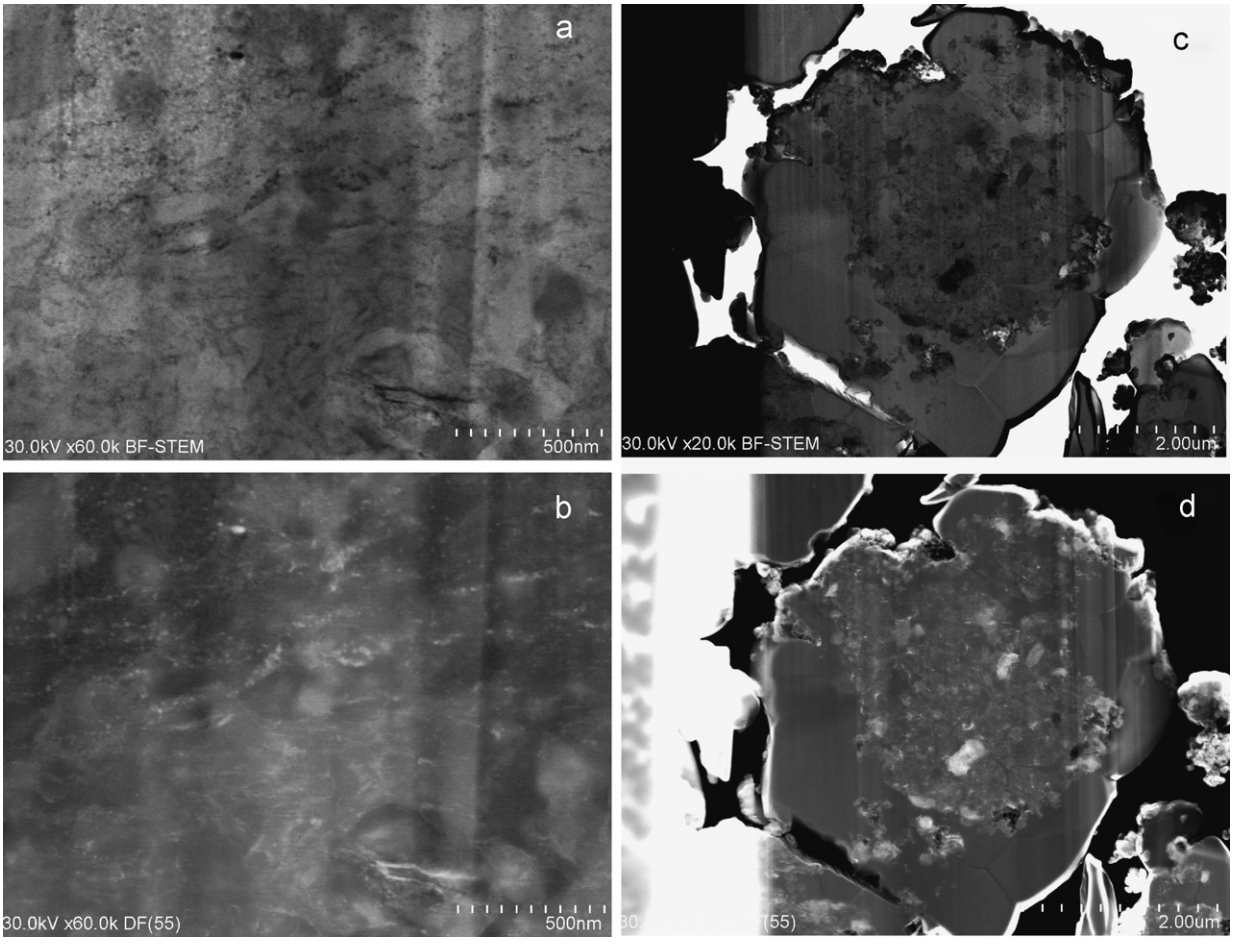

Fig. 2. Cross-sectional STEM images showing the microstructures of milled MgH_2/halide samples after 50 sorption cycles: (a) MgH_2/NbF_5 sample—BF, (b) MgH_2/NbF_5 sample—DF, (c) MgH_2/ZrF_4 sample—BF and (d) MgH_2/ZrF_4 sample—DF.

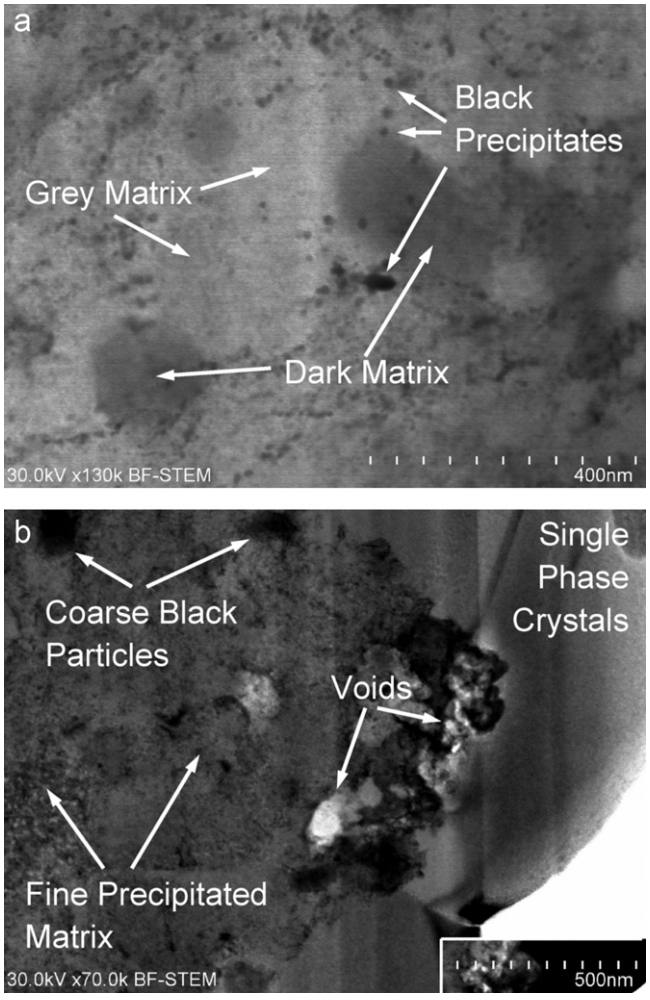

Fig. 3. Cross-sectional STEM BF images showing higher magnifications of the microstructures of samples after cyclic loading: (a) MgH_2/NbF_5 and (b) MgH_2/ZrF_4.

a level of about 4.9 wt.% of H_2 after 25 sorption cycles. A more pronounced decrease in hydrogen capacity can be observed for the MgH_2/NbF_5 sample, for which the hydrogen storage capacity stabilizes at 4.5 wt.% of H_2 after 30 sorption cycles. Furthermore, a declining hydrogen capacity for the MgH_2/NbF_5 sample after the first 10 cycles is more pronounced as compared to the MgH_2/ZrF_4 sample, which actually does not change. This essential difference in sorption behavior between the MgH_2/halide samples is due to various microstructural changes during cyclic hydriding and dehydriding at 325 °C.

The cross-sectional STEM bright and dark field (BF/DF) images of the milled MgH_2/NbF_5 and MgH_2/ZrF_4 samples after 50 sorption cycles are shown in Fig. 2. Both investigated materials clearly possess different microstructures. The MgH_2/NbF_5 sample is characterized by a multiphase structure containing black spherical precipitates, forming a plait-like structure in the mixed dark and grey matrix (Fig. 2a) under observation with the BF detector, where a relatively heavily weighted phase appears with dark contrast. Investigations of the precipitates performed with the DF detector (Fig. 2b) and at a higher magnification (Fig. 3a) reveal that the precipitates have a nanoscale dimension, mostly smaller than 20 nm in diameter. In contrast to the MgH_2/NbF_5 sample, the microstructure of magnesium hydride milled with zirconium fluoride after 50 sorption cycles is characterized by a "core and mantel" structure (Fig. 2c and d). The "core" is comprised of coarse black particles embedded in the fine precipitated matrix, while the "mantel" consists of single phase crystals with clearly visible grain boundaries often observed in the "core" region precipitations (Fig. 3b).

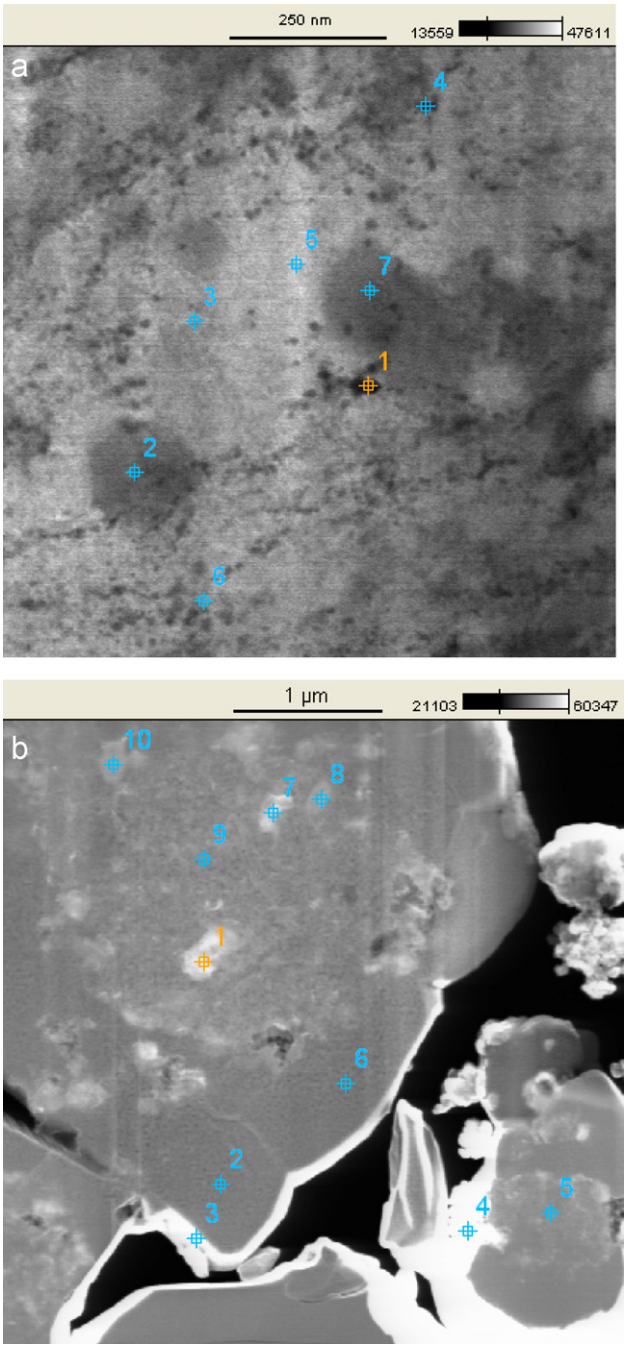

Fig. 4. BSE micrographs showing the microstructure of samples with marked points of EDS analysis: (a) MgH_2/NbF_5 and (b) MgH_2/ZrF_4. The EDS results are shown in Tables 1 and 2.

The observations of the MgH_2/NbF_5 sample carried out in the BSE detector combined with the EDS analysis revealed that there are three chemically distinguished regions of the Nb-rich black precipitates and Mg-rich grey matrix as well as the F-containing dark matrix (Fig. 4a and Table 1). The spot numbers 1, 4 and 6 in Fig. 4a and Table 1 refer to nano-sized Nb-rich black precipitates. The presence of Mg and F is not obvious in this phase because of the small size of the analyzed particles and the related problem of large measurement error. Moreover, the EDS signal can overlap the phases underneath the surface (not visible). According to the discussion in [11] the Nb-rich nano-sized precipitates are most likely

Table 1
Quantitative EDS analysis of the MgH_2/NbF_5 sample after 50 sorption cycles, taken at points as shown in Fig. 4a. The results are in at.%.

Spot number	O–K	F–K	Mg–K	Nb–L
1	5.38 ± 0.58	8.07 ± 0.79	66.71 ± 0.90	19.84 ± 0.29
2	2.39 ± 0.59	23.72 ± 1.29	72.41 ± 0.87	1.48 ± 0.24
3	3.70 ± 0.41	–	94.42 ± 1.31	1.88 ± 0.30
4	5.78 ± 0.52	4.11 ± 0.71	83.91 ± 1.10	6.21 ± 0.20
5	2.82 ± 0.43	–	97.18 ± 1.10	–
6	6.16 ± 0.70	–	89.79 ± 1.12	4.05 ± 0.29
7	3.19 ± 0.59	25.40 ± 1.27	70.00 ± 0.84	1.41 ± 0.14

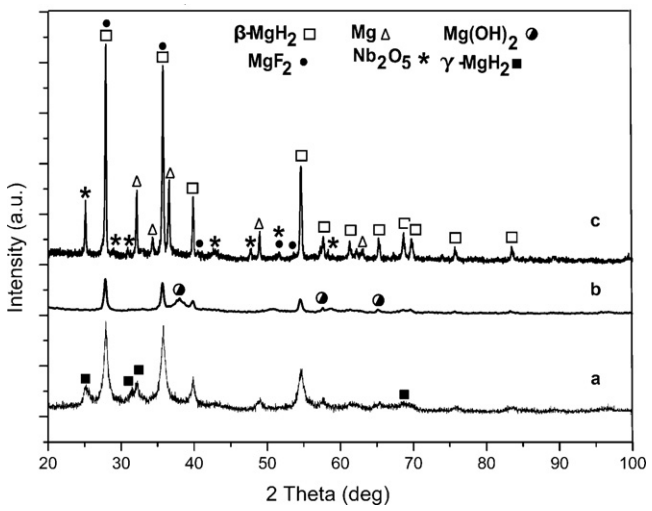

Fig. 5. XRD diffraction patterns of the $MgH_2 + NbF_5$ powder mixture after: (a) ball milling, (b) ball milling and subsequent desorption/absorption, and (c) 50 sorption cycles.

metallic Nb crystalline phase. The authors observed that during the absorption/desorption cycling of high-energy ball milled MgH_2 with NbF_5, the amorphous Nb–F layer formed after the onset of the desorption process transforms to an Nb crystalline layer covering the nano-sized MgH_2/Mg grains. The fluorine element originating from Nb–F is dissolved into MgH_2/Mg during the dehydrogenation, and the oversaturated fluorine consequently forms a separate MgF_2 phase within the desorbed MgH_2. This finding is consistent with our observations of a high content of fluorine in the dark phase (spot numbers 2 and 7 in Fig. 4a and Table 1), which may allow us to identify this phase as MgF_2. At this time, the incompatibility of the measured and stoichiometric compositions of MgF_2 is the result of the standardless method applied during measurements, which in the case of light elements and especially gases, generates large measurement errors.

Some amount of oxygen in the sample can result from the transfer of thin samples in air from the FIB to the FE SEM. The dominant "grey" areas (spot numbers 3 and 5 in Fig. 4a and Table 1) are characterized by the existence high amounts of Mg (more than 95 at.%) and barely detectable F. Therefore, the grey area can be identified as MgH_2 or locally desorbed Mg, which is explained by the fact that MgH_2 is extremely unstable under an electron beam and transforms to metallic magnesium or to an oxide.

Direct evidence of the MgF_2 formation while cycling the MgH_2/NbF_5 sample can be seen in the XRD patterns in Fig. 5. After ball milling the only diffraction peaks of an equilibrium and metastable β-MgH_2 and γ-MgH_2 phases are observed. There is no presence of the NbF_5 phase because it is in the amorphous state after ball milling [11]. Fig. 5b presents a pattern of MgH_2/NbF_5 sample after the first desorption and absorption cycle showing very weak diffraction peaks corresponding to small amount of $Mg(OH)_2$ phase. Fig. 5c shows diffraction peaks of MgH_2, Mg, MgF_2 and Nb_2O_5 confirming that the MgF_2 phase is formed while cyclic loading. The Nb_2O_5 phase is most likely formed at the surface after an intentional pre-oxidation of samples before their XRD and SEM investigations.

The obtained results lead us to the conclusion that the MgH_2/NbF_5 sample after cyclic loading consists of the MgH_2/Mg matrix with some amount of MgF_2 phase and nano-sized Nb-rich precipitates. The MgF_2 phase and Nb-rich precipitates are originally introduced by the NbF_5 additive uniformly distributed in the powder particle volume due to the low melting point of NbF_5 ($T_m = 76\,^\circ C$), which is liquefied by frictional heat during ball milling [8].

A striking discovery of the present work is that the Nb crystallite layer covering the nano-sized MgH_2/Mg grains at the beginning of the sorption cycles does not maintain its original network structure in the course of cyclic loading, and it transforms to spherical precipitates smaller than 20 nm in diameter. Moreover, the MgF_2 phase does not appear at the interface between the fluorine catalyst and MgH_2 but forms a separate MgF_2 phase with irregular oval-like regions of hundreds of nanometers within the desorbed MgH_2.

In contrast to the MgH_2/NbF_5 sample, the examination of MgH_2 with ZrF_4 after 50 sorption cycles with BSE and EDS detectors revealed large "white" particles in Fig. 4b exhibiting the presence of Mg as a major element, high levels of Zr and some amount of F (Table 2; spot numbers 1 and 7). The observed microstructural element can be identified as ZrF_4 in the MgH_2 matrix. The "core" matrix structure marked in Fig. 3b as a "fine precipitated matrix" is characterized by the presence of major element Mg, a relatively low level of F and Zr (Fig. 4b and Table 2; spot numbers 5, 8, 9 and 10). Considering the fact that the "mantel" chemical composition (Fig. 4b and Table 2; spot numbers 2 and 6) exhibits only Mg and a low content of F (Zr is barely detected), one might assume that the fine precipitated matrix consists of nano-sized ZrF_4 particles embedded in the MgH_2 matrix. However, the quantitative EDS results are affected by the "cross-section plane." The "mantel" region can be identified as a single MgH_2 phase. In order to get more insight into the presence of the phases in the MgH_2/ZrF_4 sample after ball milling and cycling an XRD analysis was carried out the results of which are shown in Fig. 6. After ball milling the only diffraction peaks of the β-MgH_2 and γ-MgH_2 phases are visible (Fig. 6a). All peaks are rather broad indicating nanocrystallinity of the phases. The ZrF_4 phase was not detected after ball milling and the first desorption/absorption cycle (Fig. 6b). The XRD pattern in Fig. 6c presents the MgH_2/ZrF_4 sample after 50 sorption cycles showing strong peaks of the α-ZrF_4 phase accompanied by the peaks of β-MgH_2. This finding clearly exhibits that the ZrF_4 phase is stable while cycling.

The obtained microstructural results are in good agreement with the sharp decrease in the hydrogen storage capacity for the MgH_2/NbF_5 sample at the onset of cyclic loading in Fig. 1. The irreversible chemical reaction between MgH_2 and NbF_5 leads to the formation of an amorphous Nb–F layer at the beginning of the sorp-

Table 2
Quantitative EDS analysis of the MgH_2/ZrF_4 sample after 50 sorption cycles, taken at points as shown in Fig. 4b. The results are in at. %.

Spot number	O–K	F–K	Mg–K	Zr–L
1	4.30 ± 0.25	3.43 ± 0.19	82.43 ± 0.48	9.84 ± 0.19
2	3.29 ± 0.14	1.06 ± 0.16	95.64 ± 0.54	–
3	7.91 ± 0.26	1.55 ± 0.30	90.54 ± 0.69	–
4	14.57 ± 0.71	–	85.43 ± 1.68	–
5	4.80 ± 0.14	1.62 ± 0.15	92.64 ± 0.50	0.94 ± 0.05
6	3.70 ± 0.16	1.62 ± 0.17	94.62 ± 0.55	0.06 ± 0.04
7	4.73 ± 0.28	3.16 ± 0.31	83.53 ± 0.47	8.58 ± 0.16
8	3.37 ± 0.15	8.93 ± 0.18	87.00 ± 0.47	0.70 ± 0.06
9	4.21 ± 0.16	3.85 ± 0.27	91.25 ± 0.50	0.70 ± 0.07
10	3.86 ± 0.14	1.84 ± 0.23	93.38 ± 0.49	0.92 ± 0.07

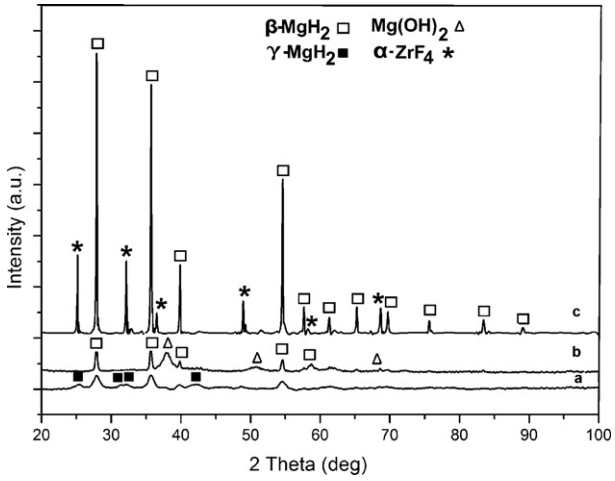

Fig. 6. XRD diffraction patterns of the $MgH_2 + ZrF_4$ powder mixture after: (a) ball milling, (b) ball milling and subsequent desorption/absorption, and (c) 50 sorption cycles.

tion cycles and finally to the Nb and MgF_2 products. The formation of the MgF_2 phase is mainly responsible for the lost of hydrogen capacity of the MgH_2/NbF_5 sample while cycling. It seems that only Nb that forms the Nb hydrides at the absorption state can act as a catalyst. The role of the MgF_2 phase is still unclear, although there are some reports suggesting that the MgF_2 surface layer has a high affinity to hydrogen [12].

In contrast, the microstructure of the MgH_2/ZrF_4 sample after cyclic loading is comprised of only MgH_2 matrix and the stable ZrF_4 additive in the "core-mantel" structure of the powder particles. This finding clearly suggests a catalytic influence of stable ZrF_4 on the MgH_2 decomposition process. Quite likely, the gradual decrease in the hydrogen storage capacity while cyclic loading for this particular material is due to some stabilization of the fraction of MgH_2/Mg with continues increase of grain size in the MgH_2/Mg regions, from about 10 nm after ball milling to hundreds of nanometers after cycling. The stabilization process makes a fraction of MgH_2/Mg inactive in the process of hydrogen desorption/absorption. The mechanism leading to that stabilization is unclear at the moment. The milling time and/or other technological parameters must be optimized in order to obtain a homogeneous distribution of the ZrF_4 phase in the volume of the MgH_2 particles after milling.

4. Conclusions

The products obtained by ball milling MgH_2/NbF_5 and MgH_2/ZrF_4 materials exhibited good hydrogen storage capacities. The hydrogen sorption stabilities evaluated using a volumetric Sieverts' apparatus showed good reversibility and performance for both materials. A better hydriding/dehydriding stability of MgH_2 modified by the ZrF_4 additive was observed while cycling at 325 °C.

The different behaviors between the two analyzed systems were related to the formation of Nb and MgF_2 phases during cyclic loading of the MgH_2/NbF_5 sample. The formation of both phases as non-uniformly distributed in the MgH_2 matrix was confirmed by microstructural observations combined with EDS and XRD analysis. The formation of the MgF_2 phase is mainly responsible for the lost of hydrogen storage capacity of the MgH_2/NbF_5 sample while cyclic loading.

In contrast, the microstructure of the MgH_2/ZrF_4 sample after cyclic loading consisted of only the MgH_2 matrix and stable nanosized ZrF_4 particles embedded in the "core" structure of powder particles. The "mantel" layer of the MgH_2/ZrF_4 particles was identified as a single crystalline MgH_2 phase. This finding clearly suggests a catalytic influence of stable ZrF_4 on the MgH_2 decomposition process. The gradual decrease in the hydrogen storage capacity while cyclic loading for this particular material is due to some stabilization of the fraction of MgH_2/Mg with continues increase of grain size in the MgH_2/Mg regions, from about 10 nm after ball milling to hundreds of nanometers after cycling. The stabilization process makes a fraction of MgH_2/Mg inactive in the process of hydrogen desorption.

Acknowledgement

This work was supported by a grant from the Polish Ministry of Sciences and Higher Education, Key Project POIG.01.03.01-14-016/08, which is gratefully acknowledged.

References

[1] R.A. Varin, T. Czujko, Z.S. Wronski, Nanomaterials for Solid State Hydrogen Storage, Springer Science + Business Media, New York, USA, 2009.
[2] B. Sakintuna, F. Lamari-Darkrim, M. Hirscher, Int. J. Hydrogen Energy 32 (2007) 1121–1140.
[3] V. Bhat, A. Rougier, L. Aymard, X. Darok, G. Nazri, J.M. Tarascon, J. Power Sources 159 (2006) 107–110.
[4] S. Deledda, A. Borissova, C. Poinsignon, W.J. Botta, M. Dornheim, T. Klassen, J. Alloys Compd. 404–406 (2005) 409–412.
[5] Y. Luo, P. Wang, L.-P. Ma, H.-M. Cheng, J. Alloys Compd. 453 (2008) 138–142.
[6] N. Recham, V.V. Bhat, M. Kandavel, L. Aymard, J.-M. Tarascon, A. Rougier, J. Alloys Compd. 464 (2008) 377–382.
[7] S.-A. Jin, J.-H. Shim, Y.W. Cho, K.-W. Yi, J. Power Sources 172 (2007) 859–862.
[8] S.-A. Jin, J.-H. Shim, J.-P. Ahn, Y.W. Cho, K.-W. Yi, Acta Mater. 55 (2007) 5073–5079.
[9] J.W. Kim, J.-P. Ahn, S.-A. Jin, S.H. Lee, H.-S. Chung, J.-H. Shim, Y.W. Cho, K.H. Oh, J. Power Sources 178 (2008) 373–378.
[10] I.E. Malka, T. Czujko, J. Bystrzycki, Int. J. Hydrogen Energy 35 (2010) 1706–1712.
[11] J.W. Kim, J.-P. Ahn, D.H. Kim, H.-S. Chung, J.-H. Shim, Y.W. Cho, K.H. Oh, Scripta Mater. 62 (2010) 701–704.
[12] F.J. Liu, S. Suda, J. Alloys Compd. 231 (1995) 742–750.